Instrument Science Report WFC3 2010-16

IR Channel Subarray Dark Current Behavior

B. Hilbert
October 28, 2010

ABSTRACT

Using data collected during Cycle 17, we have created updated dark current reference files for all IR subarray modes requested by WFC3 users during the cycle. The new files represent a significant increase in the signal-to-noise ratio of these reference files over the old versions. The reference files also show that the dark current signal in the early reads of a MULTIACCUM observation can decrease with time in certain cases. This behavior is dependent upon the timing pattern used to read out the detector, highlighting the importance of read-by-read dark current subtraction. Some of the new reference files also show the effects of "subarray banding", the source of which is currently poorly understood. Future studies should shed light on this effect.

Introduction

Throughout Cycle 17 we have collected dark current observations using all subarray modes requested by WFC3 users. Similar to what was done to create the full-frame dark current reference files (Hilbert & McCullough, 2009), we collected these data and used them to produce a mean dark current observation for each subarray mode. These files can now be used by the community to achieve a high quality dark current subtraction as part of their data reduction.

Data

We used dark current ramps collected throughout Cycle 17 to construct these updated dark current reference files. Calibration programs 11929 and 12097 were used to collect dark current ramps with all of the array sizes and sample sequences requested by observers during the cycle. This will enable all observers to perform dark current subtraction on their data using on-orbit based dark current data. For the purposes of creating dark current files, we collect data in the same manner as described for the full frame dark current data in WFC3 ISR 2009-21 (Hilbert & McCullough, 2009). At each requested sample sequence and array size, we collected a series of data ramps. Each ramp was composed of 16 non-desctructive readouts of the IR detector, taken while the filter wheel had the BLANK positioned in the beam. These data were then combined following the procedure outlined in the Data Reduction section below in order to create the reference files.

List of Observations

Table 7 in the Appendix lists the files used in the construction of the subarray dark current reference files. Table 1 below lists, for each subarray, the number of files used to create the dark current reference file, along with a note of whether subarray banding is visible in the new reference file. Subarray banding is discussed in the Analysis section below, and will be presented in more detail in a future report.

Data Reduction

Each individual dark current ramp was processed through the same data reduction steps used in the creation of the latest full-frame dark current references files (Hilbert &McCullough, 2009). All MULTIACCUM ramps (with each ramp composed of 16 non-desctructive reads of the detetor) were run through the *calwf3* version 2.1 data reduction pipeline with only the DQICORR, ZOFFCORR, BLEVCORR, CRCORR, and UNITCORR steps turned on. Taken together, these steps remove the overall bias level and pixel-to-pixel bias variations from the data, import a copy of the bad pixel table into each file (Hilbert & Bushouse, 2010), and convert the output *ima* and *flt* files to units of DN and DN per second, respectively. See the Chapter 3 of the WFC3 Mini-Data Handbook (Quijano et al., 2009) for details on *calwf3* processing steps.

After processing the individual ramps through *calwf3*, the creation of the dark current reference file for a given array size/sample sequence combination was a straight forward process. We simply took the individual ramps and calculated sigma-clipped mean signal values on a pixel-by-pixel and read-by-read basis, in order to produce a mean 16-read dark current ramp. Note that since the zeroth read subtraction was performed during the data reduction steps described above, the zeroth read of the mean ramp is composed entirely of zeros. Mean values were calculated using IDL's *resistant_mean.pro* with a 3-

σ clipping limit. This mean ramp is then delivered to the calibration database system (CDBS) for use as a reference file to be used in future data calibration.

Sample Sequence	Array Size (pixels)	Banding Present in Superdark	Number of Files Used
RAPID	64 x 64	No	28
	128 x 128	No	28
	256 x 256	No	28
	512 x 512	Yes	28
SPARS10	128 x 128	Yes	28
	256 x 256	Yes	28
	512 x 512	No	5
SPARS25	256 x 256	Yes	28
	512 x 512	Yes	28
STEP25	512 x 512	Yes	28
SPARS100	256 x 256	No	5
	512 x 512	No	5
SPARS200	256 x 256	No	5
	512 x 512	No	4

***Table 1**: The number of files used to create each dark current reference file, along with a note on whether subarray banding is present in the final reference file.*

Analysis

Appearance and Comparison to Full Frame Darks

Figure 1 shows an image of the mean dark current measured in this work. In order to create the image, we took the 16-read dark current reference file and performed line-fitting on each pixel's signals up through the 16 reads of the ramp. By collecting the best-fit slopes from this line fitting, we produced a dark rate image. This is similar to the line-fitting that is performed as one of the final steps in standard *calwf3* processing, where the output signal rate image is saved in the *flt* file. The elevated signal-to-noise of this rate image versus that of a single read in the original dark current reference file allows for a clearer image of the large scale dark current behavior.

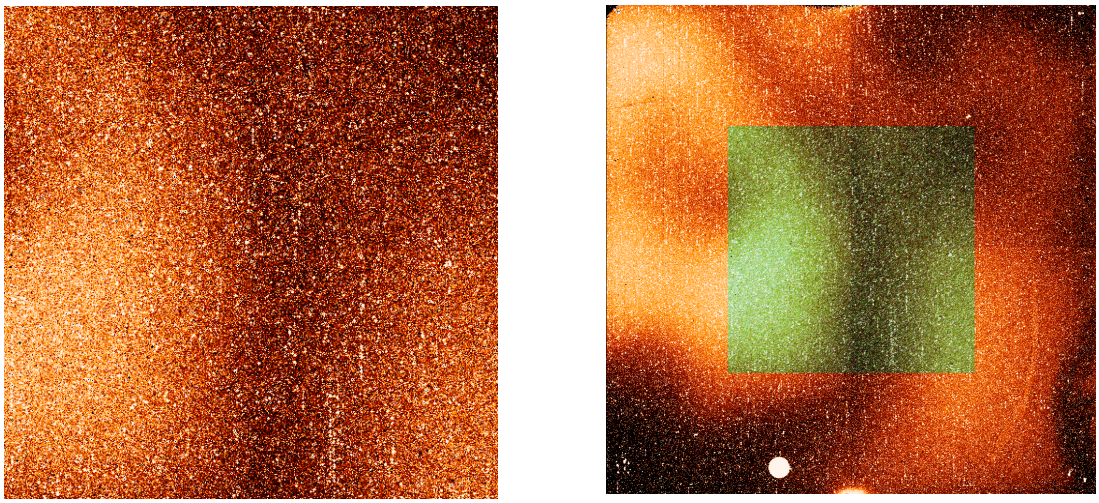

Figure 1*: (Left panel) Dark current in the 512 x 512 subarray using the SPARS200 sample sequence. (Right panel) The same 512 x 512 subarray dark image (green) overlaying the full-frame SPARS200 dark current image (red, from WFC3 ISR 2009-21) at the actual location on the detector from which the subarray data are collected. The green subarray image has also been made semi-transparent, allowing the central portion of the red full frame image to show through. Note the very similar large scale structure of the two images. This implies that the dark current behavior of the detector is unchanged between full frame and subarray modes. All images are displayed with a histogram equalization stretch with values from 0 to 0.4 DN/sec.*

The left panel of Figure 1 shows the dark rate measured in the 512 x 512 pixel subarray when using the SPARS200 sample sequence (total exposure time: 2771.7 seconds). The pattern and level of dark current seen here is very similar to that visible in the central 512 x 512 pixels of the full frame SPARS200 CDBS dark current image

(*u4819494i_drk.fits*). An image of this full frame dark current file is shown as Figure 3 in WFC3 ISR 2009-21 and reproduced in the right panel of Figure 1. Here, the central green square is the same 512 x 512 subarray dark current image seen in the left panel. We positioned this image on top of an image of the full frame SPARS200 dark current, at the location corresponding to the area used when observing with a 512 x 512 subarray. By making the subarray image semi-transparent, the central 512 x 512 pixels in the red full frame image can also been seen. From the clarity in the central 512 x 512 region, along with the lack of only red or only green areas, we see that the dark current behavior in the central 512 x 512 pixels is similar regardless of whether the data are collected in full frame or subarray mode.

Given the apparent consistency in the central 512 x 512 pixels' dark current behavior, one may ask whether subarray dark current subtraction could be performed simply by extracting the appropriate subarray from the full frame dark current reference file. Unfortunately, it appears that this is not an ideal solution, for two reasons. First, the subarray banding issue, described in greater detail below, is an effect that can create a significant difference between the subarray data and full frame data.

Secondly, while the dark current rate images in the right panel of Figure 1 are very similar, a closer look at the data reveals differences between full frame and subarray data in the signals measured in the non-destructive reads which comprise the ramp. Figure 2 shows an example of this. The green line in this figure shows the mean signal measured in all 16 reads of the 512 x 512 pixel SPARS200 dark ramp. These are the reads on which line-fitting was performed in order to arrive at the image in the left panel of Figure 1. The blue line shows the mean signal measured in the central 512 x 512 pixels in all 16 reads of the full frame SPARS200 dark current reference file.

Note that line fitting (ignoring the first two reads) will result in very similar dark rates (slopes) for the two lines, as implied in the right panel of Figure 1. However, looking read-by-read, we see that there is a significant difference between the absolute signal in the full frame versus that in the subarray as the ramp progresses. The reset effects present in the first two reads are different for the two array sizes, causing an offset between the two lines. There is also a small difference between the slopes of the lines. These differences show that we need to have a separate dark current reference file for the subarray, rather than extracting a subarray from the full frame file, in order to obtain the best calibration.

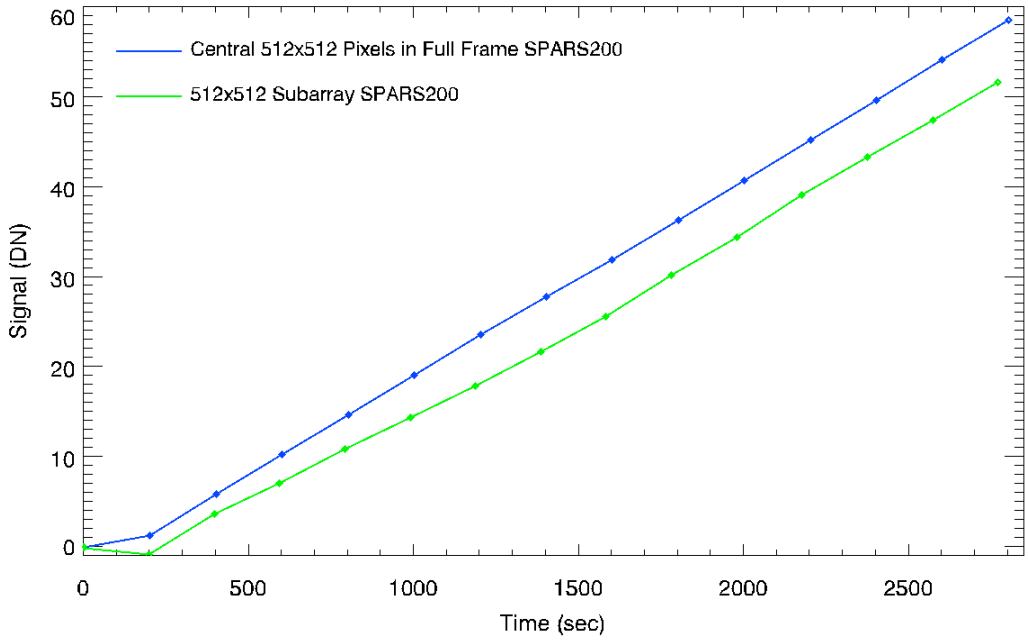

Figure 2*: Plot of the mean signal in each of the 16 reads for both the 512 x 512 pixel subarray SPARS200 dark current file, as well as the central 512 x 512 pixels in the full frame SPARS200 dark current reference file. Reset effects early in the ramps as well as slight differences in the slopes result in significantly different signals measured along the ramps.*

Dark Current Statistics

Basic characterizations of the new dark current reference files are presented below. Prior to the delivery of these new dark current files to CDBS, many of the array size/sample sequence combinations did not have dark current calibration files (beyond placeholder files containing all zeros) in CDBS. For those combinations that did have a previous calibration file in place (all of which were derived from ground testing data), we compare the new on orbit-derived dark current files to the old file. Table 6 in the Appendix lists the CDBS filenames of both the newly created dark current reference files and the previous versions created from ground testing data.

Although Figure 2 shows that using dark current rate images can hide potentially significant effects, for ease of comparison we present below some statistics from the dark rate images created from the new dark current reference files rather than from the actual 16-read ramps themselves.

Table 3 shows the sigma clipped mean and robust standard deviation (from IDL's *resistant_mean.pro* and *robust_sigma.pro*, respectively) across the entire subarray for all sample sequence and array size combinations. Note that the most useful comparisons to

make in this table are of the values for the old versus new version of a given subarray. Since the various subarray sizes sample different populations of pixels and (as seen in the right panel of Figure 1) the dark current behavior varies on large spatial scales, it is not useful to compare the mean or standard deviation values across subarrays of different sizes. Similarly, comparing mean values and standard deviations between similarly-sized subarrays with different sample sequences is difficult due to the large variation in exposure times, and therefore signal-to-noise. For sample sequences that are long enough for the dark current signal to begin to dominate over readnoise, such as the SPARS100 and SPARS200 sequences, one can see that the mean dark current rates become independent of sample sequence.

Sample Sequence	Array Size (pix)	Mean (DN/sec)	Robust Stdev	Previous Files: Mean	Previous File: Stdev
RAPID	64	-0.9321	1.5792	-1.0453	3.4228
	128	-0.4365	0.8271	-0.4984	1.8515
	256	-0.1407	0.3359	-0.1651	0.7602
	512	-0.0345	0.1128	-0.0310	0.2522
SPARS10	128	0.0088	0.0155	0.0141	0.0331
	256	0.0234	0.0200	0.0258	0.0351
	512	0.0144	0.0324	0.0160	0.0308
SPARS25	256	0.0229	0.0063	NA	NA
	512	0.0213	0.0092	NA	NA
STEP25	512	0.0081	0.0081	NA	NA
SPARS100	256	0.0192	0.0045	NA	NA
	512	0.0207	0.0045	NA	NA
SPARS200	256	0.0194	0.0032	NA	NA
	512	0.0203	0.0036	NA	NA

***Table 3**: Robust mean and standard deviations for the dark current rates measured in the new and previous versions of dark current reference files.*

Figures 3 and 4 provide a graphical view of the values in the table above. These figures show histograms of the dark current signal rate in the SPARS200 512 x 512 and SPARS10 256 x 256 subarrays, respectively. In the case of the SPARS10 data, the red line shows the histogram for the new dark current rate image, while the blue line shows the histogram derived from the previous version of this dark reference file. By combining 28 ramps compared to the 6 ramps used to create the previous version, the resulting dark current rate image has a higher signal to noise ratio. There is no previous

version of the SPARS200 512 x 512 dark current file, which is why only a single histogram is present in Figure 3.

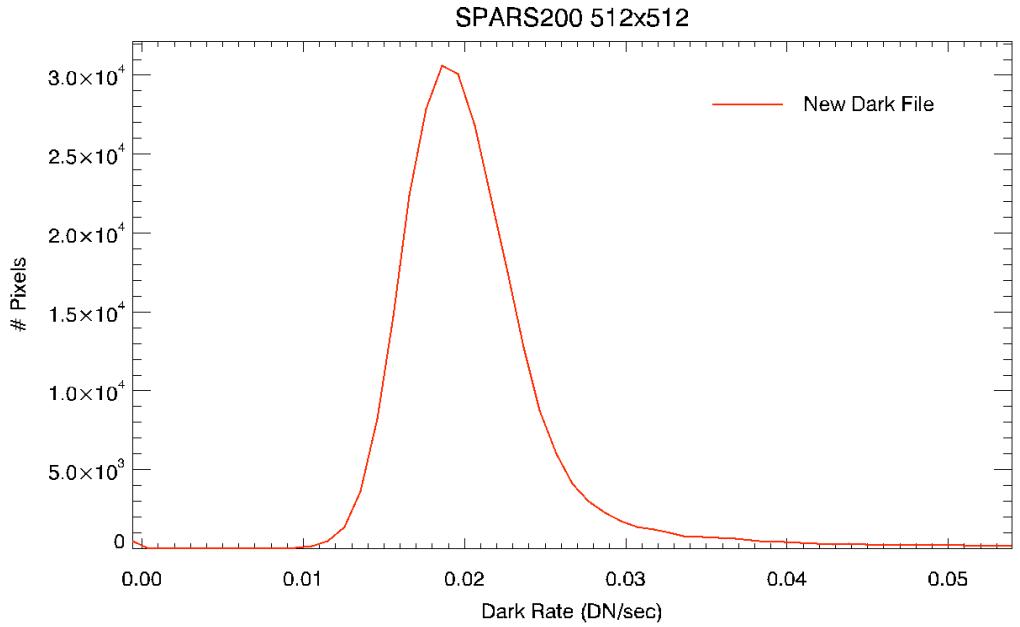

***Figure 3**: Histogram of dark current rates in the new SPARS200 512 x 512 subarray reference file.*

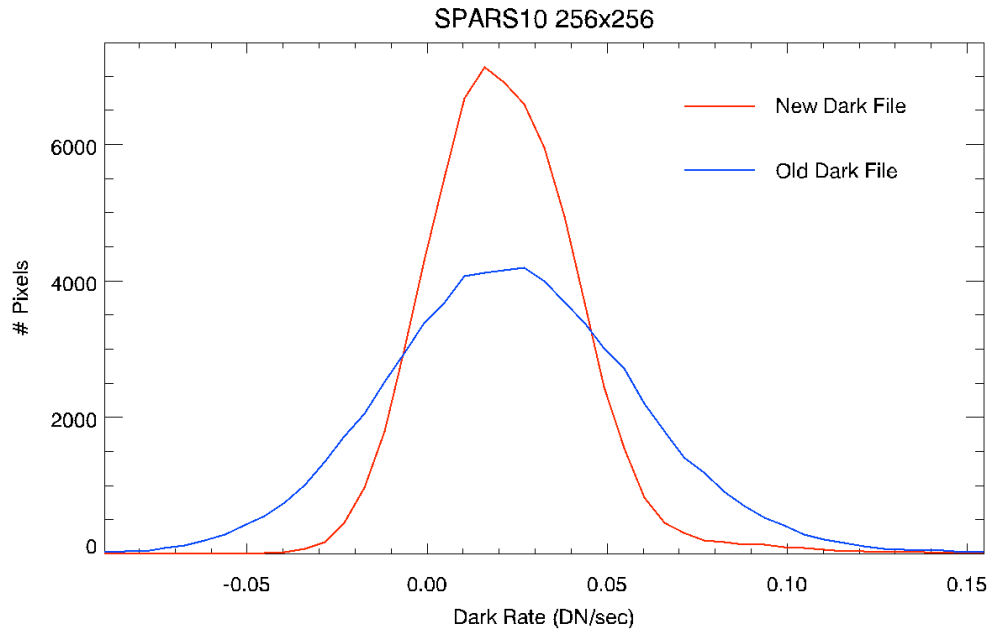

***Figure 4**: Histograms of dark current rates in the new and old SPARS10 256 x 256 subarray reference files. The improved signal-to-noise in the new file versus the old is due to the larger number of ramps used to create the mean.*

Read-by-Read Dark Behavior

To better understand the dark current behavior in the subarray files, as well as any differences between the new files and those that had previously been in place, we had to inspect the dark current files on a read-by-read basis. Previous investigations (Hilbert, 2008, Hilbert and McCullough, 2009) have found that the dark current signal does not necessarily increase linearly with time. Instead, detector reset effects have been shown to cause a *decrease* in dark current signal in the early reads of ramps, followed by a reversal to a positive dark current rate later in the ramp. This can be seen in Figure 2. The magnitude and timescale associated with the negative dark current has been observed to vary with sample sequence. Figures 2 and 3 in WFC3 ISR 2008-30 (Hilbert, 2008), give further details.

Figure 5 below shows the mean signal measured in each of the 16 reads of the new dark current reference file (red line) as well as the previous version (blue line). The large negative signal jump between 0 and 7.5 seconds occurs in all individual SPARS10 256 x 256 ramps. The magnitude of this jump has a robust standard deviation of 0.1 DN, implying that the red and blue data points at a time of 7.5 seconds are statistically identical within the error bars.

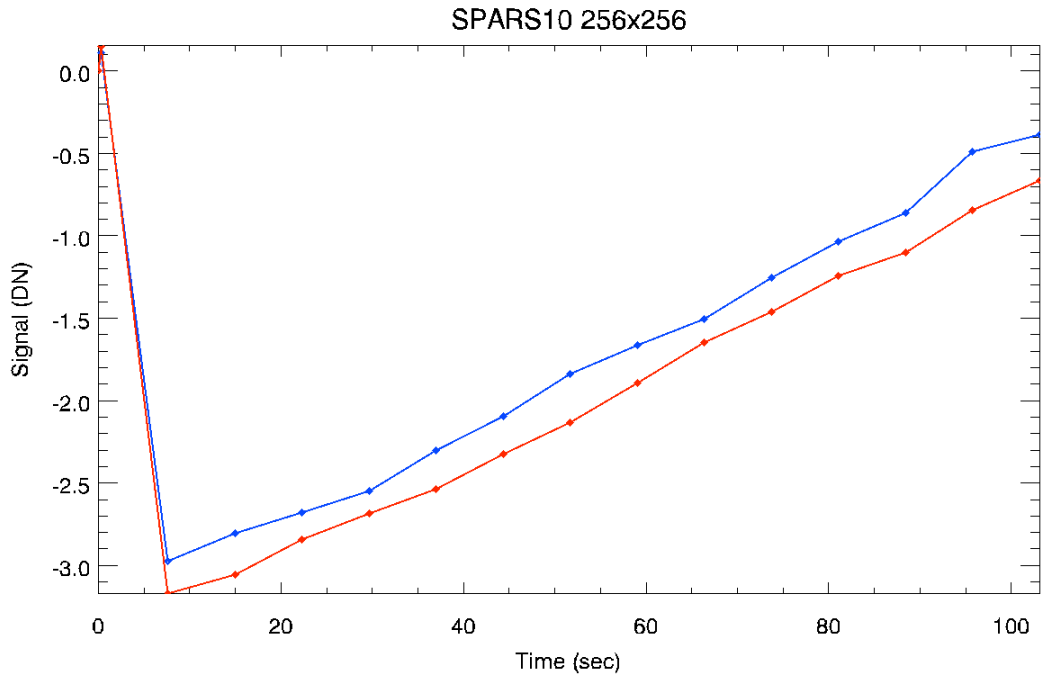

Figure 5*: Mean signal in all 16 reads for the new dark current reference file (red) as well as the previous version (blue).*

Figure 6 shows that the magnitude and timing of this negative signal jump varies with sample sequence. This figure shows the mean dark current signal up the ramp (offset by + 3DN for ease of plotting on a log scale) for all 6 of the new 512 x 512 subarray dark current reference files. This plot shows that in the first ~200 seconds of a ramp, the dark current behavior is highly dependant on sample sequence. Note that in the case of a RAPID ramp (black line), the dark current is always negative. That is, the slope of the line is negative, and the measured signal decreases throughout the ramp. Also note that the STEP25 ramp matches this behavior for the first 5 reads, during which the readout pattern is identical to that for the RAPID ramp. After the 5th read, the amount of time between readouts increases, and the dark current responds with a large negative jump. This plot illustrates the importance of creating a separate dark current reference file for each sample sequence and array size through dedicated observations, rather than creating such a file by simply scaling a master dark current frame by exposure time.

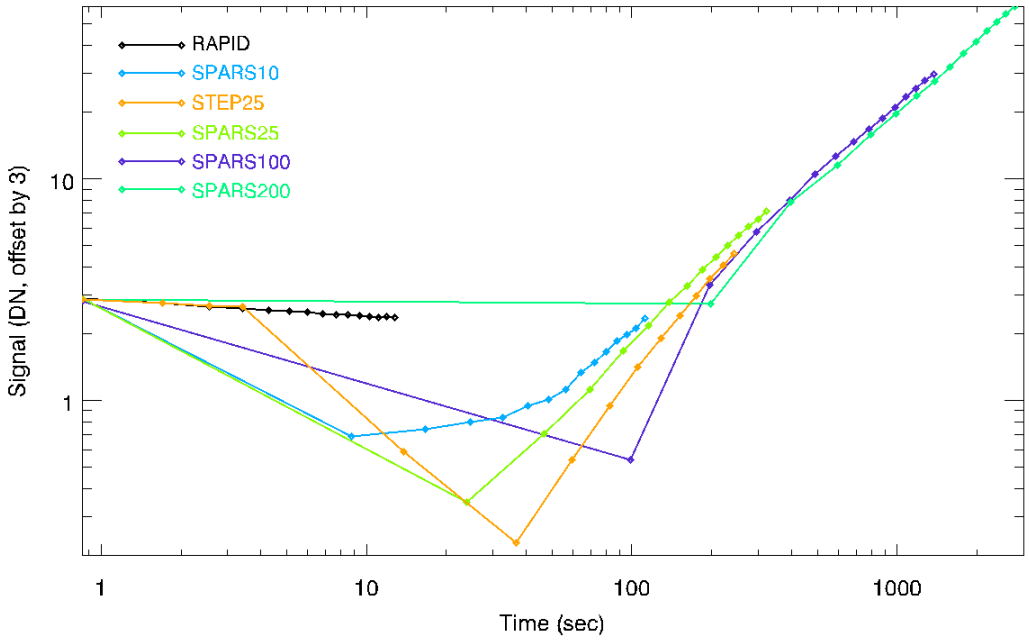

***Figure 6**: Plot showing the mean dark current behavior up the ramp for all of the new 512 x 512 subarray dark current reference files.*

Along with the creation of mean dark current signals when creating these new reference files, we also focused on creating an up-to-date list of hot pixels, which is presented in the data quality arrays associated with each file. In order to identify hot

pixels, we relied on the signal rate image created from the mean signal ramp of the SPARS200 512 x 512 subarray. We produced a dark current rate image for this file by performing line-fitting on the measured signals up the ramp. We then flagged as hot any pixels with measured dark current rates greater than 0.4 e^-/sec. This is the same threshold as was used when searching the full frame data for hot pixels. We then copied this hot pixel mask into the data quality arrays for each of the subarray files, extracting the appropriate subarray when necessary. The hot pixels are flagged with a value of 16 in the data quality arrays of the reference files. Table 4 lists the percentage of active pixels flagged as hot for each subarray size.

Array Size	% Hot
64	0.71%
128	0.71%
256	0.67%
512	0.64%

Table 4*: Percentage of active pixels in each subarray size flagged as hot in the new versions of the dark current reference files. The high signal-to-noise SPARS200 512x512 reference file was used to identify hot pixels and create a hot pixel mask. The appropriate areas of this mask were then extracted and copied into the lower signal-to-noise reference files.*

Subarray Banding

As mentioned above, certain sample sequence/array size combinations suffered from what we call "subarray banding". This feature, with an as-yet unknown cause, appears as a horizontal band across the central portion of the detector, within which the signal level is depressed relative to the top and bottom areas of the detector. Investigations into the source of this behavior, as well as the development of methods to mitigate it, are ongoing.

Figure 7 shows the dark current rate for the 256 x 256 pixel subarray when using the SPARS10 sample sequence (total exposure time: 103.1 seconds), as well as for the 512 x 512 pixel SPARS25 subarray. These subarray observing modes are two of those more strongly affected by subarray banding, as can be seen by the dark band across the center of the images. To give an idea of the magnitude of the effect, when comparing the dark current signal in the final read of the ramp used to produce the image on the left in Figure 7, we found that the mean signal outside the band was -0.72 DN, while that inside the band was -2.91 DN.

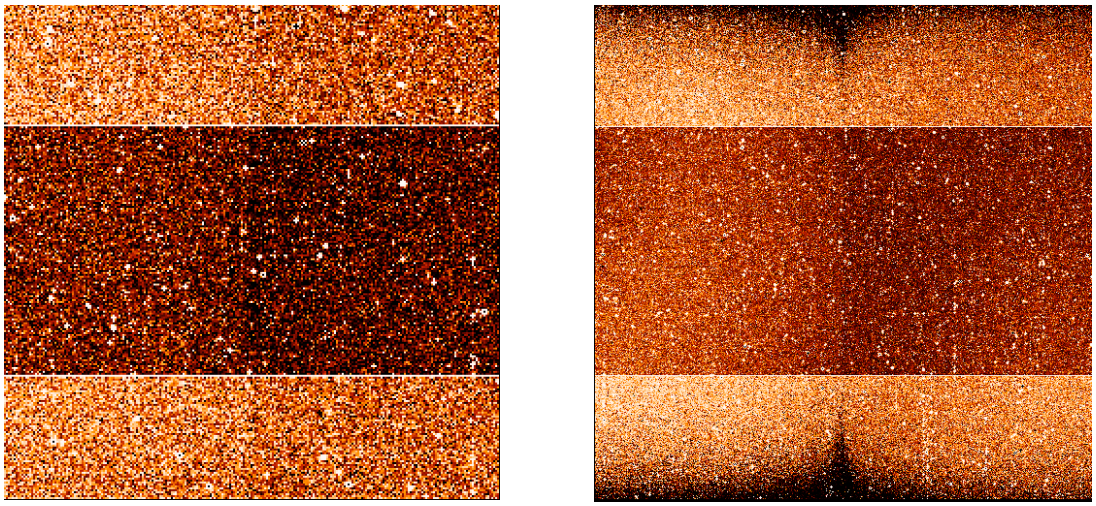

Figure 7*: (Left panel) Dark current image for the SPARS10 256 x 256 subarray. (Right panel) Dark current image for SPARS25 512 x 512 subarray, scaled down to fit next to the 256 x 256 image. Both images are shown with a histogram equalization stretch running from 0 to 0.4 DN/sec. The darker band running horizontally through the images is the subarray banding feature discussed in the text. The cause of this banding is still under investigation.*

Figure 8 shows more quantitatviely the effects of the banding, using the file that produced the image in the right panel above. The blue line in Figure 8 shows the mean signal in each of the 16 reads up the ramp for pixels located outside of the central band. The green line shows the mean signals for pixels inside of the band. Note that a large fraction of the difference between the two lines occurs in reads 1 and 2, which occur 0.85 and 23.8 seconds after the initial (zeroth) read. The rest of the difference in signal appears to come from a reduced dark rate (seen as a flatter slope) in the pixels inside the band. The causes behind this banding effect are still under investigation.

We have measured the magnitude of the subarray banding in the new dark current reference files, and report it in Table 5. For each of the sample sequence/subarray size combinations listed in Table 1 as displaying the subarray banding, we calculated two mean signals in the final read of the new reference file. The first mean was that of the pixels outside the subarray band. This value is reported in the rightmost column of Table 5. We then calculated the mean signal in the pixels within the subarray band. The second column from the right gives the difference in DN between the signal outside of the band and that within. Pixels in the central band always display depressed signals relative to those in the pixels outside the band.

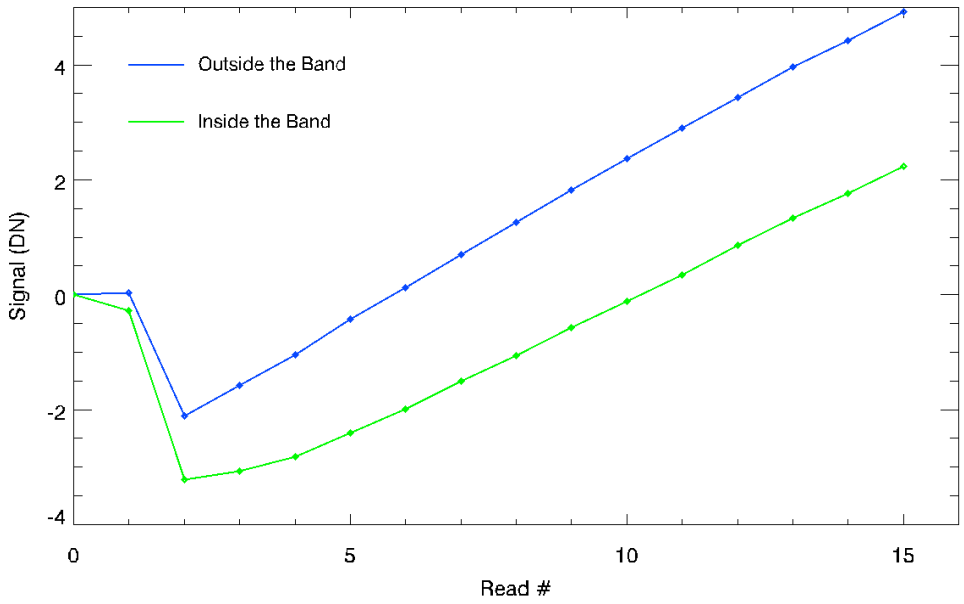

***Figure 8**: Measured mean dark current signal in all of the 16 reads up the ramp. The blue curve shows the mean signal for pixels located above and below the banding, while the green curve shows the mean signals for the pixels within the central band.*

Sample Sequence	Array Size	Signal Difference in Final Read, Outside Band Minus Inside Band (DN)	Mean Signal Outside the Band in the Final Read (DN)
RAPID	512	0.37	-0.52
SPARS10	128	0.62	-4.11
SPARS10*	256	3.54	0.71
SPARS25	256	0.79	2.26
SPARS25*	512	2.65	4.87
STEP25	512	0.29	1.27

***Table 5**: Magnitude of the subarray banding in the new dark current reference files. We calculated the mean signal value in the pixels located outside of the band (rightmost column), as well as for those pixels inside of the band, in the final read of the ramp. The second column from the right shows the difference in DN between the mean signal outside versus inside the band. The two files with the largest banding amplitude are marked with stars above and shown in Figure 7.*

Conclusions

New dark current reference files have been created for all Cycle 17 user-requested subarray modes. These files represent the first on-orbit derived subarray dark current reference files, and represent a significant improvement in signal-to-noise over the previous versions of these files.

Measured dark current is very similar, although not identical, to that measured in the full frame dark current files taken in Cycle 17. Dark current behavior up the ramp shows that optimal dark current subtraction can only be done with subarray dark current files, rather than extraction of the appropriate subarray from a full frame dark current file.

Reset effects are significant in the early reads of all dark current ramps. These effects vary with sample sequence and can dominate the overall dark current signal in low signal-to-noise dark current observations.

Subarray banding also has significant effects on signal level for those modes where it has been seen to exist. Ongoing investigations should provide indications of whether or not this phenomenon is preventable, at which time we may be able to remove the banding from the dark current reference files.

Recommendations

Observers should pay careful attention to their dark current subtraction strategy. For those with data where dark current signal is insignificant, it is possible that skipping the dark current subtraction step is worthwhile, especially in the cases where dark current subtraction may imprint the subarray banding into data which previously did not exhibit that effect.

References

Hilbert, B., ***WFC3 TV3 Testing: IR Channel Dark Current.*** WFC3 ISR 2008-30. http://www.stsci.edu/hst/wfc3/documents/ISRs/WFC3-2008-30.pdf Sept 2008.

Hilbert, B. and H. Bushouse, ***WFC3/IR Bad Pixel Table: Update Using Cycle 17 Data***. WFC3 ISR 2010-13. http://www.stsci.edu/hst/wfc3/documents/ISRs/WFC3-2010-13.pdf August 2010.

Hilbert, B. and P. McCullough. ***WFC3 SMOV Program 11420: IR Channel Functional Tests***. WFC3 ISR 2009-23. http://www.stsci.edu/hst/wfc3/documents/ISRs/WFC3-2009-23.pdf June 2009.

Hilbert, B. and P. McCullough. ***WFC3 SMOV Results: IR Channel Dark Current, Readnoise, and Background Signal***. WFC3 ISR 2009-21. http://www.stsci.edu/hst/wfc3/documents/ISRs/WFC3-2009-21.pdf June 2010.

Kim Quijano, J., et al. 2009, "WFC3 Mini-Data Handbook", Version 1.0, (Baltimore: STScI)

Appendix

Sample Sequence	Array Size (pixels)	New Dark Current Reference File	Previous File
RAPID	64	uaf12559i_drk.fits	t5s1754ei_drk.fits
	128	uaf12556i_drk.fits	t5s1754bi_drk.fits
	256	uaf12557i_drk.fits	t5s1754ci_drk.fits
	512	uaf12558i_drk.fits	t5s1754di_drk.fits
SPARS10	128	uaf1255ci_drk.fits	t5s1754ji_drk.fits
	256	uaf1255di_drk.fits	t5s1754ki_drk.fits
	512	uaf1255ei_drk.fits	t5s1754li_drk.fits
SPARS25	256	uaf1255hi_drk.fits	NA
	512	uaf1255ii_drk.fits	NA
STEP25	512	uaf1255ji_drk.fits	NA
SPARS100	256	uaf1255ai_drk.fits	NA
	512	uaf1255bi_drk.fits	NA
SPARS200	256	uaf1255fi_drk.fits	NA
	512	uaf1255gi_drk.fits	NA

Table 6*: List of filenames for the new and old subarray dark current reference files. Previous files listed as NA existed only as a placeholder file (containing all zeroes) in CDBS prior to this update.*

***Table 7**: List of all files used in the creation of the new subarray dark current reference files.*

Sample Sequence	Array Size (pixels)	Files
RAPID	64 x 64	ibcu0dk0q, ibcu0qk4q, ibcu12i0q, ibcu1dfzq, ibcu1qi1q, ibcu25jeq, ibcu2di6q, ibcu2qgqq, ibcu38nsq, ibcu3dh7q, ibcu3qftq, ibcu4dh7q, ibcu4qgmq, ibcu51r8q, ibcu5dzbq, ibcu5qwaq, ibcu64iaq, ibcu6dy7q, ibcu6qxwq, ibcu77noq, ibcu7dw5q, ibcu7qacq, ibcu8dweq, ibcu8qdfq, ibcu90h9q, ibcu9dfmq, ibcu9qa5q, ibcua3gxq
	128 x 128	ibcu0djxq, ibcu0qk1q, ibcu12hxq, ibcu1dfwq, ibcu1qhyq, ibcu25jbq, ibcu2di3q, ibcu2qgnq, ibcu38npq, ibcu3dh4q, ibcu3qfqq, ibcu4dh4q, ibcu4qgjq, ibcu51r5q, ibcu5dz8q, ibcu5qw7q, ibcu64i7q, ibcu6dy4q, ibcu6qxtq, ibcu77nlq, ibcu7dw2q, ibcu7qa9q, ibcu8dwbq, ibcu8qdcq, ibcu90h6q, ibcu9dfjq, ibcu9qa2q, ibcua3guq
	256 x 256	ibcu0djyq, ibcu0qk2q, ibcu12hyq, ibcu1dfxq, ibcu1qhzq, ibcu25jcq, ibcu2di4q, ibcu2qgoq, ibcu38nqq, ibcu3dh5q, ibcu3qfrq, ibcu4dh5q, ibcu4qgkq, ibcu51r6q, ibcu5dz9q, ibcu5qw8q, ibcu64i8q, ibcu6dy5q, ibcu6qxuq, ibcu77nmq, ibcu7dw3q, ibcu7qaaq, ibcu8dwcq, ibcu8qddq, ibcu90h7q, ibcu9dfkq, ibcu9qa3q, ibcua3gvq
	512 x 512	ibcu0djzq, ibcu0qk3q, ibcu12hzq, ibcu1dfyq, ibcu1qi0q, ibcu25jdq, ibcu2di5q, ibcu2qgpq, ibcu38nrq, ibcu3dh6q, ibcu3qfsq, ibcu4dh6q, ibcu4qglq, ibcu51r7q, ibcu5dzaq, ibcu5qw9q, ibcu64i9q, ibcu6dy6q, ibcu6qxvq, ibcu77nnq, ibcu7dw4q, ibcu7qabq, ibcu8dwdq, ibcu8qdeq, ibcu90h8q, ibcu9dflq, ibcu9qa4q, ibcua3gwq
SPARS10	128 x 128	ibcu0dk1q, ibcu0qk5q, ibcu12i1q, ibcu1dg0q, ibcu1qi2q, ibcu25jfq, ibcu2di7q, ibcu2qgrq, ibcu38ntq, ibcu3dh8q, ibcu3qfuq, ibcu4dh8q, ibcu4qgnq, ibcu51r9q, ibcu5dzcq, ibcu5qwbq, ibcu64ibq, ibcu6dy8q, ibcu6qxxq, ibcu77npq, ibcu7dw6q, ibcu7qadq, ibcu8dwfq, ibcu8qdgq, ibcu90haq, ibcu9dfnq, ibcu9qa6q, ibcua3gyq

	256 x 256	ibcu0dk2qibcu0qk6q, ibcu12i2q, ibcu1dg1q, ibcu1qi3q, ibcu25jgq, ibcu2di8q, ibcu2qgsq, ibcu38nuq, ibcu3dh9q, ibcu3qfvq, ibcu4dh9q, ibcu4qgoq, ibcu51raq, ibcu5dzdq, ibcu5qwcq, ibcu64icq, ibcu6dy9q, ibcu6qxyq, ibcu77nqq, ibcu7dw7q, ibcu7qaeq, ibcu8dwgq, ibcu8qdhq, ibcu90hbq, ibcu9dfoq, ibcu9qa7q, ibcua3gzq
	512 x 512	ibed11g9q, ibed12jdq, ibed13k2q, ibed14keq, ibed15knq
SPARS25	256 x 256	ibcu0dk4q, ibcu0qk8q, ibcu12i4q, ibcu1dg3q, ibcu1qi5q, ibcu25jiq, ibcu2diaq, ibcu2qguq, ibcu38nwq, ibcu3dhbq, ibcu3qfxq, ibcu4dhbq, ibcu4qgqq, ibcu51rcq, ibcu5dzfq, ibcu5qweq, ibcu64ieq, ibcu6dybq, ibcu6qy0q, ibcu77nsq, ibcu7dw9q, ibcu7qagq, ibcu8dwiq, ibcu8qdjq, ibcu90hdq, ibcu9dfqq, ibcu9qa9q, ibcua3h1q
	512 x 512	ibcu0dk5q, ibcu0qk9q, ibcu12i5q, ibcu1dg4q, ibcu1qi6q, ibcu25jjq, ibcu2dibq, ibcu2qgvq, ibcu38nxq, ibcu3dhcq, ibcu3qfyq, ibcu4dhcq, ibcu4qgrq, ibcu51rdq, ibcu5dzgq, ibcu5qwfq, ibcu64ifq, ibcu6dycq, ibcu6qy1q, ibcu77ntq, ibcu7dwaq, ibcu7qahq, ibcu8dwjq, ibcu8qdkq, ibcu90heq, ibcu9dfrq, ibcu9qaaq, ibcua3h2q
STEP25	512 x 512	ibcu0dk6q, ibcu0qkaq, ibcu12i6q, ibcu1dg5q, ibcu1qi7q, ibcu25jkq, ibcu2dicq, ibcu2qgwq, ibcu38nyq, ibcu3dhdq, ibcu3qfzq, ibcu4dhdq, ibcu4qgsq, ibcu51req, ibcu5dzhq, ibcu5qwgq, ibcu64igq, ibcu6dydq, ibcu6qy2q, ibcu77nuq, ibcu7dwbq, ibcu7qaiq, ibcu8dwkq, ibcu8qdlq, ibcu90hfq, ibcu9dfsq, ibcu9qabq, ibcua3h3q
SPARS100	256 x 256	ibed16kwq, ibed17t8q, ibed18tgq, ibed19tuq, ibed20umq
	512 x 512	ibed11gaq, ibed12jcq, ibed13k3q, ibed14kdq, ibed15kmq
SPARS200	256 x 256	ibed01tlq, ibed02tzq, ibed03u8q, ibed04udq, ibed05veq
	512 x 512	ibed07fkq, ibed08k0q, ibed09epq, ibed10f0q